Propulsion System Design, Optimization, Simulation, and Testing for a Long-Endurance Solar-Powered Unmanned Aircraft

Or D. Dantsker* and Marco Caccamo [†]

Technical University of Munich, Garching, Germany

Saym Imtiaz[‡]

University of Illinois at Urbana–Champaign, Urbana, IL 61801

In recent years, we have seen an uptrend in the popularity of UAVs driven by the desire to apply these aircraft to areas such as precision farming, surveying and mapping, search and rescue missions, and more. A major technical hurdle to overcome is that of drastically reducing the overall power consumption of these UAVs so they can be powered by solar arrays, and for long periods of time. The propulsion system plays a critical part in the overall power consumption of the UAV and therefore, it is necessary to determine the most optimal combination of possible propulsion system components for a given mission profile, i.e. propellers and motors. Hundreds of options are available for each of the components with generally non-scientific advice for choosing the proper combinations. A computationally-intensive, long-endurance solar-powered unmanned aircraft, the UIUC-TUM Solar Flyer is currently in development to enable a variety of all-daylight hour missions to be performed, involving continuous acquisition and processing of high resolution imagery. Currently, the critical choice has becomes what propulsion system components to use. A previously-developed mission-based propulsion system optimization tool and fixed-wind, electric unmanned aircraft propulsion system power model was used in this paper to select optimal combinations of possible components, i.e. propellers and motors, for the UIUC-TUM Solar Flyer, given a typical mission profile. Specifically, the optimization tool was able to match a motor-propeller combination that was 19% more efficient relative to the baseline (previously in use) combination for the given mission profile thrust and velocity design point. This paper first provides an overview of propulsion system optimization tool and system power model, including details regarding their validation. Then, recent wind tunnel performance testing of folding propellers is presented along with key observations. Next, a mission profile for the UIUC-TUM Solar Flyer was simulated and the resulting thrust and velocity design point are input into the propulsion system optimization tool to determine an optimally matched motor-propeller combination. Finally, a summary is given and future work is discussed.

Nomenclature

ESC	=	electronic speed controller	$\vec{F}$	=	force vector
MPPT	=	maximum power point tracker	g	=	gravitational acceleration
RPM	=	rotations per minute	i_m	=	motor current
UAV	=	unmanned aerial vehicle	i_0	=	zero load motor current
			J	=	advance ratio
$\vec{a}$	=	aircraft acceleration vector	K	=	aerodynamic constant
C_{D_o}	=	zero-lift drag coefficients	K_i, K_p	=	propulsion model constants
C_P	=	power coefficient	K_v	=	motor speed constant
C_T	=	thrust coefficient	m	=	aircraft mass
D	=	propeller diameter, drag	n	=	propeller and motor rotation rate

---

*Researcher, Department of Mechanical Engineering, AIAA Student Member.

[†]Professor, Department of Mechanical Engineering.

[‡]Undergraduate Student, Department of Aerospace Engineering.

American Institute of Aeronautics and Astronautics

P	=	power		v	=	velocity
P_{ESC}	=	ESC output power		$\vec{v}$	=	velocity vector
P_{motor}	=	motor output power		W	=	weight
$P_{propulsion}$	=	propulsion power consumption				
P_{thrust}	=	aerodynamic thrust power from propeller		γ	=	climb angle
Q	=	torque		η_{motor}	=	motor efficiency
R_m	=	internal motor resistance		$\eta_{propeller}$	=	propeller efficiency
S	=	wing area		ϕ	=	roll (bank) angle
T	=	thrust		ρ	=	density of air
U_m	=	motor terminal voltage				

I. Introduction

In recent years, we have seen an uptrend in the popularity of UAVs driven by the desire to apply these aircraft to areas such as precision farming, infrastructure and environment monitoring, surveillance, surveying and mapping, search and rescue missions, weather forecasting, and more. The traditional approach for small size UAVs is to capture data on the aircraft, stream it to the ground through a high power data-link, process it remotely (potentially off-line), perform analysis, and then relay commands back to the aircraft as needed.[1–3] Given the finite energy resources found onboard an aircraft (battery or fuel), traditional designs greatly limit aircraft endurance since significant power is required for propulsion, actuation, and the continuous transmission of visual data. All the mentioned application scenarios would benefit by carrying a high performance embedded computer system to minimize the need for data transmission. A major technical hurdle to overcome is that of drastically reducing the overall power consumption of these UAVs so that they can be powered by solar arrays. The process of reducing aircraft power consumption is required to reduce the aircraft weight, prolong flight time, and ultimately reduce cost in order to support the widespread adoption of UAVs for different types of missions.

Limited on-board energy storage significantly limits flight time and ultimately the usability of unmanned aircraft. The propulsion system plays a critical part in the overall energy power consumption of the UAV. Therefore, it is necessary to determine the most optimal combination of possible propulsion system components for a given mission profile, i.e. propellers and motors. Hundreds of options are available for each of the components with generally non-scientific advice for choosing the proper combinations. To date, there has been significant effort in the modeling[4–7] and testing[8–22] of UAV propulsion system components. However, there has been comparatively limited effort put into optimizing the matching of these components,[23] rather mostly towards custom-designed or generic-shaped propellers.[24–28]

Currently, the UIUC-TUM Solar Flyer, which is shown in Fig. 1, is in development to enable a variety of all-daylight hour missions to be performed, involving continuous acquisition and processing of high resolution imagery. The aircraft is instrumented with an integrated uavAP autopilot,[29] and high-fidelity Al Volo data acquisition system[30] with an integrated 3D graphics processing unit (GPU). In order to keep the aircraft relatively inexpensive, both in labor and cost, the aircraft has been developed using a majority of commercial-off-the-shelf components, which therefore highly limits the number of viable options. The airframe chosen for development was selected through trade studies [31] that considered airframe availability and payload requirements as well as potential energy collection — more detail regarding airframe selection and integration can be found in related literature.[31–33] The critical choice in the UIUC-TUM Solar Flyer's development has become what propulsion system components to use. A previously-developed mission-based propulsion system optimization tool[34] and fixed-wind, electric unmanned aircraft propulsion system power model[35] was used in this paper to select the most optimal combinations of possible components, i.e. propellers and motors, for the UIUC-TUM Solar Flyer given a typical mission profile.

American Institute of Aeronautics and Astronautics

Figure 1: The UIUC-TUM Solar Flyer aircraft.

This paper first provides an overview of the fixed-wind, electric unmanned aircraft propulsion system power model, including simulated and experimental flight testing validation. This is followed by an overview of the mission-based propulsion system optimization tool, including functional process diagrams and flight testing validation. Recent wind tunnel performance testing of folding propellers is then presented along with a description of observations. Next, a mission profile for the UIUC-TUM Solar Flyer is presented and simulated yielding a thrust and velocity design point for the propulsion system. After that, the propulsion system optimization tool is used to determine an optimally matched motor-propeller combination. Finally, a summary is given and future work is discussed.

II.   Modeling and Optimization Methodology

On an electric UAV, the propulsion system is made up of a series of components. These include the electronic speed controller, motor, and propeller. Each of the components contribute to an efficiency loss, eventually converting electrical/chemical energy into mechanical work that propels the aircraft. For the scope of the present work, only the choice of the motor and propeller are considered as the choice of the electronic speed controller (ESC) is not expected to significantly affect the entire system efficiency [a]. Below, an analytical model for an electric UAV propulsion system is presented and then applied into an optimization tool, which in later sections of this paper will be applied to the UIUC-TUM Solar Flyer.

---

[a]There have been a variety of derivations developed for computing ESC efficiency.[4,19,21] These generally suggest that ESC efficiency is a function of voltage and current. Duty cycle, which is proportional to shaft rotation rate and/or throttle input, is often also taken into account. For the scope of the current work, ESC efficiency will be fixed to a constant value, which is representative of its efficiency at cruise conditions, i.e. ESC efficiency curves have shown to flatten out once reaching a small percentage of their design operating current.[19]

American Institute of Aeronautics and Astronautics

A.   Propulsion System Modeling

A power model for electric, fixed-wing unmanned aircraft was developed that produces high-fidelity power consumption estimation while requiring minimal computation. Previous works have separately looked at aircraft power modelling[36–41] and propulsion system modelling[9, 11, 42–44] with varying degrees of assumptions and verification. Compared to existing works, the propulsion power model developed below provides a more holistic approach to UAV propulsion power modelling and has been validated through flight testing. The complete derivations of this model can be found in previous literature.[35, 45]

The power model uses propulsion system modelling of the propeller and motor as well as aircraft power modelling using flight mechanics derivations; Figure 2 shows a high level diagram of the power model. In order to enable rapid computation, the resulting expression has been limited to using only measurable aircraft state variables, propulsion system parameters and curves, and (scalar) constants. The final expression for the developed power model is:

$$P_{propulsion} = \frac{K_p v^3 + K_i \frac{\cos^2 \gamma}{v \cos^2 \phi} + mgv \sin \gamma + m \vec{a} \cdot \vec{v}}{\eta_{propeller} \cdot \eta_{motor}} \tag{1}$$

$\eta_{propeller}$ is the propeller efficiency, η_{motor} is the motor efficiency, and K_p and K_i are scalar constants; these scalar constants can be determined from aircraft specifications, per the expressions below, or can be learned from training data using linear regression with a non-linear kernel. The expression for these scalars are

$$K_p = \frac{1}{2} \rho S C_{D_o} \tag{2}$$

$$K_i = \frac{2 K m^2 g^2}{\rho S} \tag{3}$$

where K is a constant aerodynamic coefficient based on the wing platform shape[b].
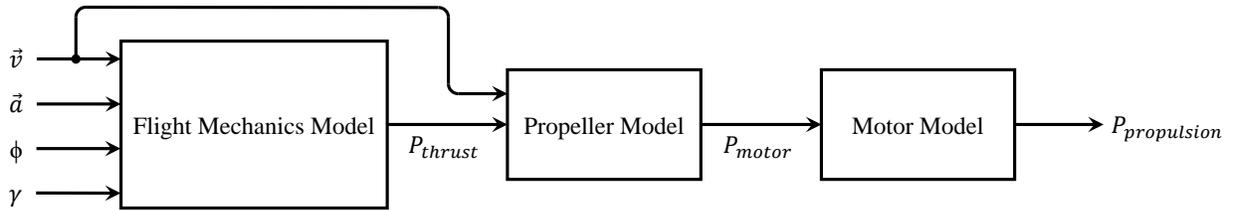
Figure 2: Aircraft propulsion power modeling based on aircraft state.

Propeller efficiency can be derived using blade element momentum theory (BEMT) and sectional airfoil theory as performed in other work.[46] However, BEMT curves are highly sensitive to variation of the parameters used. In order to increase model accuracy, experimental data for propeller performance can be obtained from wind tunnel propeller testing[9, 47] and/or an existing database,[48, 49] with interpolation being done as required; the latter technique is in use in this work. The process of determining the propeller efficiency for each given flight state follows the method presented in the following sub-section.

The motor efficiency for a brushless DC-motor can be calculated analytically using the relation between motor terminal voltage U_m and shaft rotation rate n and a variety of fixed motor parameters. A first order approximation[50] is given as

$$\eta_{motor}(n, U_m) = \left(1 - \frac{i_0 R_m}{U_m - n/K_v} \right) \frac{n}{U_m K_v} \tag{4}$$

---

[b]$K = 1/\pi e_0 AR$, where e_o is the Oswald efficiency factor and AR is the wing aspect ratio.

American Institute of Aeronautics and Astronautics

where i_0 is motor current at zero load, R_m is motor internal resistance and K_v is motor speed constant. A second order approximation[51] also exists, however, it requires a fourth motor parameter, K_Q, the motor torque constant, which is not easily obtained from manufacturers but instead needs to be measured through dynamometer benchtop testing.[21]

The resulting power model was previously evaluated by means of flight testing[35] using an existing, instrumented unmanned aircraft, the Avistar UAV, which had extensively been used for avionics development as well as other purposes.[52–55] The aircraft was autonomously flown using the uavAP autopilot[29] through a reference flight path, which contained turns, climbs, descents, and straight line segments. The flight testing showed very close agreement between the power and energy estimates determined using the power model from aircraft state data and actual experimental power and energy measurements. Additionally, using the uavEE emulation environment,[56] the reference flight path was also flown using the same autopilot and a simulated radio control model aircraft trainer, which was very similar to the one used in experimental flight testing. These flight paths are displayed in Figure 3. The flight path was nearly identical with the exception of 2 corners, where in experimental flight testing, light wind gusts deviated the aircraft slightly. The power and energy data generated was in close agreement with the experimental data as can be seen in Figure 4. The significance of this result is that the propulsion power model that was developed is able to accurately estimate the power consumption of an electric UAV based on flight path state, without needing precise aerodynamic measurements or estimation, e.g. angle-of-attack. Therefore, power estimation can be done with minimal computation.
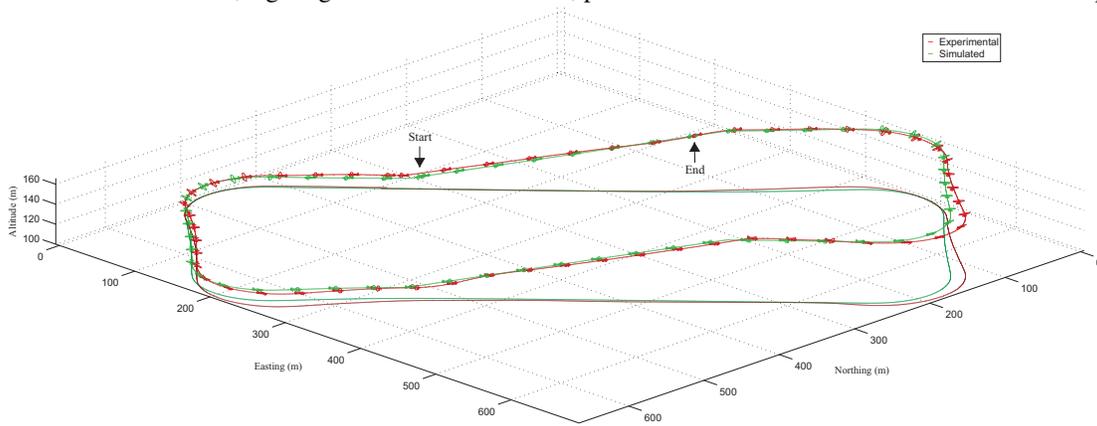
Figure 3: Comparison of aircraft path for experimental (red) and simulated flight (green) results; the airplane is plotted at 6x scale and every 2 seconds.
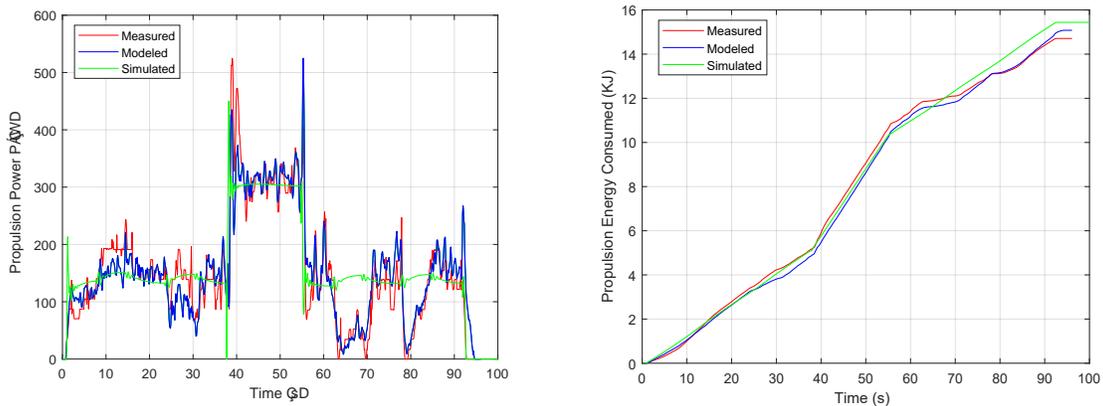
Figure 4: Comparison of (a) propulsion power and (b) energy consumed from experimental measured (red), experimental modeled (blue), and simulated (green) results using the propulsion power model.

American Institute of Aeronautics and Astronautics

B. Optimization

A propulsion system optimization tool was developed that determines (matches) the optimal propeller and motor combination(s) for an electric, fixed-wing unmanned aircraft, given desired mission requirements, i.e. it determines the combination(s) that provide the required thrust at the greatest operational efficiency, i.e. using the least amount of power. Specifically, missions are broken down into expected segments with velocity and thrust requirements being computed using an aircraft power model. The optimization tool then estimates the required propeller rotation rate and then power consumption for each segment and propeller-motor combination. It then integrates the segment results into missions for each combination and tabulates the results, sorting by overall efficiency. Process diagrams explaining how the propulsion optimization occurs are found below in Figs. 5-7. An example input set of propeller performance curves can be found in the next section. Among a variety of additional functionality integrated into the tool, the optimizer considers aircraft safety by estimating maximum thrust each combination can produce, which is crucial in upset recovery scenarios such as stall. A more detailed derivation and description of functionality can be found in previous related work.[34]

Experimental validation testing of the optimization tool was performed through flight testing of the aforementioned existing aircraft, the Avistar UAV. Due to practical limitations, the validation testing used the existing aircraft motor, the AXI 4120/14, and a choice of APC propeller[57] as they are readily available, low cost, and have been previously performance tested.[48] The optimization tool was then applied to determine the combination(s) that would be the most efficient in 20 m/s level flight, assuming a thrust requirement of 3, 4, or 5 N (the estimated required thrust). The results presented in Figure 8 show 6 propellers that provide the greater efficiency than the default propeller, the APC 13×8 E; however, only one, the APC 11×10 E, provides sufficient thrust available at the stall speed of the test aircraft for a reasonable margin of safety in flight testing. Thus, the APC 11×10 E was the sole propeller chosen for a flight testing comparison.

The aircraft was manually piloted in straight and level flight at approximately 20 m/s with the AXI 4120/14 motor and the APC 13×8 E and APC 11×10 E, respectively. To minimize environmental effects, the aircraft was tested only in calm conditions. The fligh test data was filtered for flight segments of at least 5 seconds with zero control input, minimal pitch and roll (< 5 deg), minimal climb rate (< 0.5 m/s), and near-constant propeller rotation rate (< ±100 RPM), yielding 5 data points for each of the two propellers [c]. The average voltage and current measurements (measured at the ESC providing motor power consumption) were used to compute the *measured power* while the averaged airspeed and propeller rotation rate measurements were used to compute the *computed thrust* and *computed power* using the optimization tool core functions. To confirm that the aircraft aerodynamics and thrust required has not changed by changing the propeller, the computed thrust was plotted against the measured airspeed for the two tested combinations in Fig. 9, confirming good agreement between the two combinations. Interestingly, there is a trend where thrust required decreases as the airspeed increases. This is explained by the fact that the aircraft is operating slower than its peak efficiency.[58]

Fig. 10 shows the computed thrust plotted against the measured airspeed for the two combinations. The results showed that the optimized AXI 4120/14 motor and APC 11×10 E propeller combination requires approximately ***20% less power*** than the default combination. There are similar trends for the measured and computed power requirements within each combination, however, there are decently large deviations especially at lower speeds. The majority of deviations can be explained by instrument measurement uncertainty. Specifically, the instrumentation used in-flight is only able to measure propeller rotation rate and airspeed within an accuracy of ± 100 RPM and ± 0.5 m/s, respectively. The measured results are plotted with error bars for velocity offsets (as rotation rate measurement error do not effect their values) while the computed results are plotted with error bar boundaries for the rotation rate and velocity offsets. 9

---

[c]In total, 5 data points were measured for each of the two propeller, each averaged from thousands of individual airspeed, propeller rotation rate, voltage, current samples logged at 400 Hz.

American Institute of Aeronautics and Astronautics

out of 10 measured data error bars overlap with computed data error bar boundaries signifying good agreement between the measured and computed power data when considering uncertainty.

Additionally, propulsion system optimization of potential missions was performed in simulation. The simulated missions, which included a 1 *km* by 1 *km* field coverage flight (described in Section IV) and a 6-site inspection flight about an 8 *km²* area, showed the advantage of using mission optimized propeller-motor combinations with significant efficiency gains of **50% to 75%** relative to the default combination. Performing these propulsion system optimization are especially paramount for long-endurance and/or solar-powered aircraft.
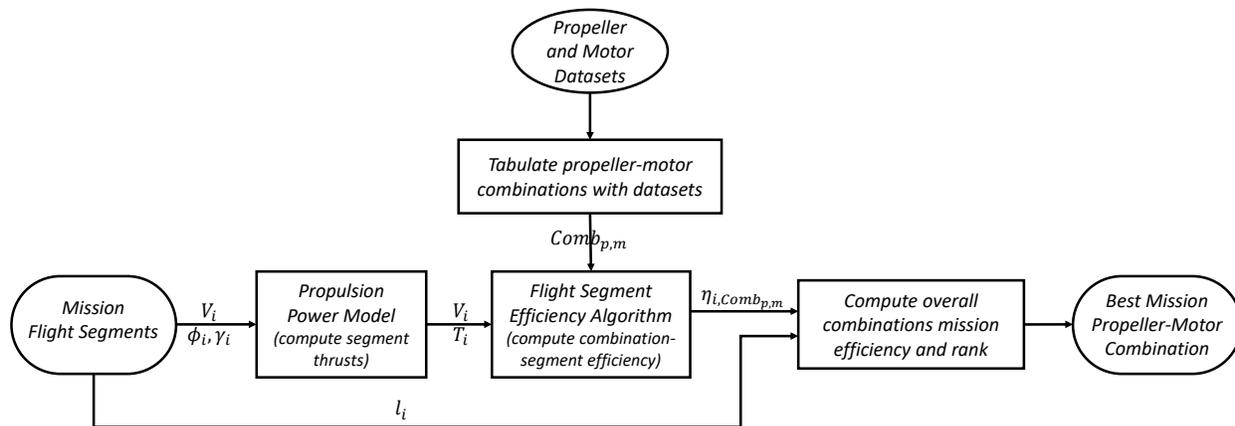
Figure 5: Process diagram for the *Mission Based Propulsion System Optimization*.
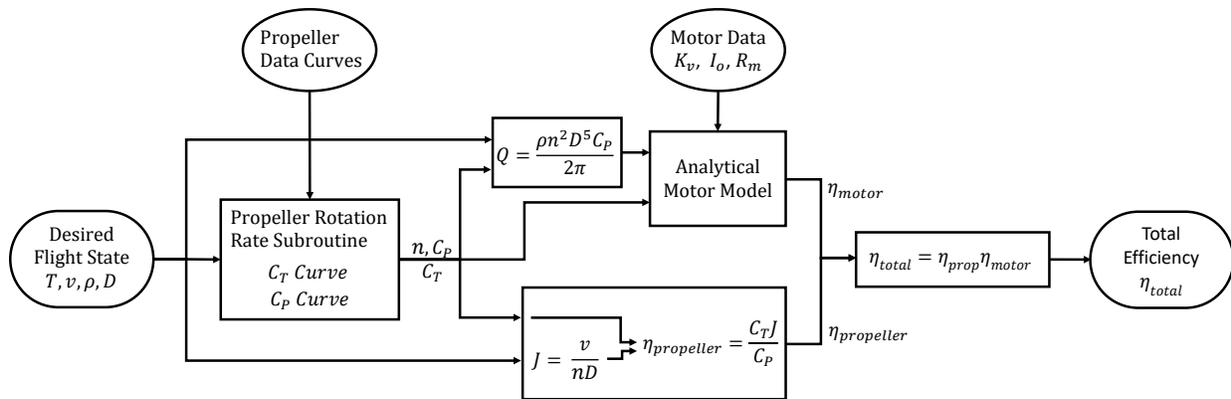
Figure 6: Process diagram of the *Flight Segment Propeller-Motor Efficiency Algorithm.*

American Institute of Aeronautics and Astronautics

```
                    ┌─────────┐
                    │  Begin  │
                    └────┬────┘
                         ▼
        ┌────────────────────────────┐
        │  Initialize the two closest │
        │      $C_T$ and $n$ values   │
        └──────────────┬─────────────┘
                       ▼
              ╱ Any $C_T$ ╲        ┌─────┐
             ⟨  curves?    ⟩──────▶│ End │
              ╲           ╱  false └─────┘
                  │ true
                  ▼
        ┌────────────────────────┐ ◀──────┐
        │   Initialize current $n$ │        │
        └──────────┬─────────────┘          │
                   ▼                         │
        ┌────────────────────────┐          │
        │      Calculate J        │          │
        │   $J = \dfrac{v}{nD}$   │          │
        └──────────┬─────────────┘          │
                   ▼                         │
        ┌────────────────────────┐          │
        │   Interpolate for $C_T$ │          │
        └──────────┬─────────────┘          │
                   ▼                         │
        ┌────────────────────────┐          │
        │ Calculate expected $C_T$│          │
        │ $C_T = \dfrac{T}{\rho n^2 D^4}$ │  │
        └──────────┬─────────────┘          │
                   ▼                         │
        ┌────────────────────────┐          │
        │  Update the two closest │          │
        │    $C_T$ and $n$ values │          │
        └──────────┬─────────────┘          │
                   ▼                         │
              ╱   Any    ╲                   │
             ⟨ remaining  ⟩─────── true ─────┘
              ╲ $C_T$ curves? ╱
                   │ false
                   ▼
        ┌────────────────────────┐
        │ Interpolate between the two │
        │  closest $C_T$ polars for $n$ │
        └──────────┬─────────────┘
                   ▼
        ┌────────────────────────┐
        │   Interpolate for $C_P$ │
        └──────────┬─────────────┘
                   ▼
              ┌─────────┐
              │   End   │
              └─────────┘
```

Figure 7: Process diagram of the *Propeller Rotation Rate Subroutine*.
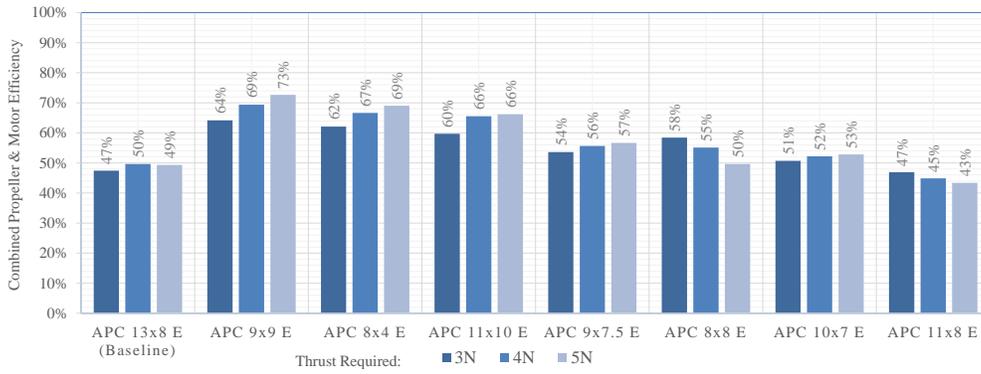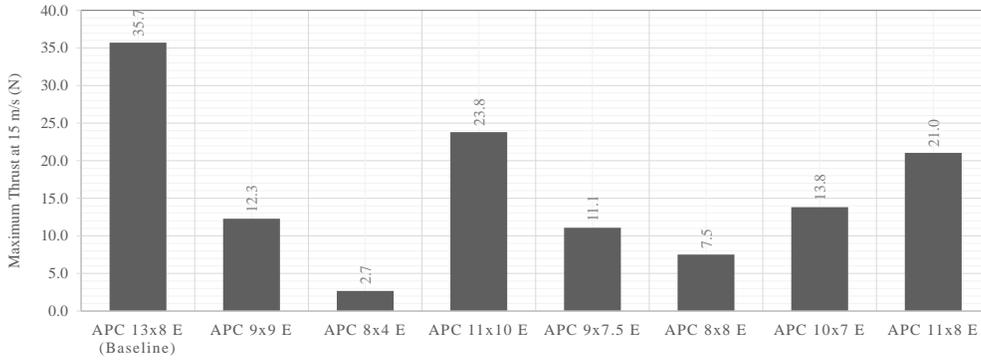
Figure 8: Comparison of (a) motor propeller efficiency for required thrusts of 3, 4, and 5 *N* at 20 *m/s* and (b) the maximum thrust available at 15*m/s* for AXI 4120/14 motor with various APC E propellers.
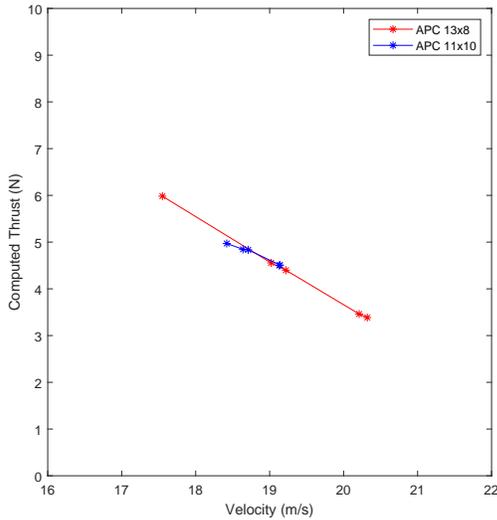
Figure 9: Computed thrust vs. measured airspeed for the AXI 4120/14 motor and the APC 13×8 E and APC 11×10 E, respectively, in straight and level flight with the Avistar UAV.
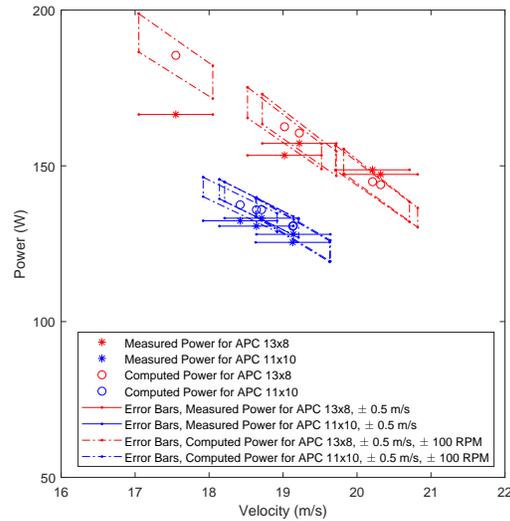
Figure 10: Measured and computed power consumption vs. measured airspeed for the AXI 4120/14 motor and the APC 13×8 E and APC 11×10 E, respectively, in straight and level flight with the Avistar UAV.

American Institute of Aeronautics and Astronautics

III. Wind Tunnel Propeller Testing

Propeller performance testing of 40 Aero-Naut CAM carbon propellers in 2-blade configuration was conducted in March 2020 at the UIUC low-turbulence subsonic wind tunnel to provide a dataset for optimization of the UIUC-TUM Solar Flyer propulsion system.[47] Based on examination of existing long endurance aircraft, Aero-Naut CAM carbon folding propellers,[59] which are shown in Fig. 11, were chosen for testing as these propellers are well known throughout the UAV industry.[60–63] As the Aero-Naut CAM 13×6.5 propeller was actively being used on the UIUC-TUM Solar Flyer and was found to be oversized for the desired aircraft performance, Aero-Naut CAM folding propellers with diameters (D) of 9 to 13 in and a variety of pitches (P) were tested. However, for completeness, 14 to 16 in CAM folding propellers, which are closer to the range of propeller sizes recommended by the airframe manufacturer, were also tested to show that these larger blade propellers are indeed oversized for the UIUC-TUM Solar Flyer. Table 1 lists the specific diameters and pitches for the propellers that were tested.

Figure 11: A photo of several Aero-Naut CAM carbon folding propeller blades (taken from Aero-Naut[59]).

Table 1: List of Aero-Naut CAM Carbon Folding Propellers Tested

Aero-Naut CAM Carbon Folding Propellers								
9×4	10×4	11×4	12×5	12.5×6	13×5	14×6	15×6	16×6
9×5	10×5	11×6	12×6	12.5×7	13×6.5	14×8	15×8	16×8
9×6	10×6	11×7	12×6.5	12.5×9	13×8	14×9	15×10	
9×7	10×7	11×8	12×8		13×10	14×12		
	10×8	11×10	12×9		13×11			
	10×12	11×12	12× 10					
			12× 13					

American Institute of Aeronautics and Astronautics

Propeller tests were conducted using a propeller testing balance adapted and validated to several previous works.[9,13,64] In this testing setup, propeller performance was measured using a thrust and torque balance. Thrust was measured outside of the tunnel test section using a T-shaped pendulum balance that pivoted about two flexural pivots and was constrained on one side by a load cell. The torque from the propeller was measured using a reaction torque sensor placed between the motor sting and the support arm of the thrust balance. To remove the torque cell, motor sting, balance support arm, and any wires from the propeller slipstream and test section velocity, a fairing surrounded the setup. The fairing spanned the test section from the floor to the ceiling in order to keep the test section flow symmetric. The motor sting was long enough for all the propellers to be more than 1.5 diameters from the fairing in order to minimize the effect of the fairing on the propeller performance. Propeller RPM was measured by shining a red laser through the propeller disc area to a phototransistor. As the propeller spun, the propeller blades blocked the laser beam, and the receiver output voltage dropped to around zero. During the tests, the propellers were driven by a brushless electric motor using a electronic speed controller (ESC). The propeller blades were mounted to the motor using a 2-bladed, 40mm diameter Aero-Naut Folding Turbo spinner using a 42 mm diameter Aeronaut yoke; this hinged mounting setup is identical to the one used on the UIUC-TUM Solar Flyer and that allows the blades to freely rotate forwards/backwards. To simplify the laboratory setup, a 1500 W power supply was used to power the motor and speed controller instead of using batteries. To set the rotational speed of the motor, the speed controller was connected to a modified servo controller, which relayed throttle commands from the data acquisition computer. More information regarding the wind tunnel testing equipment, calibration, data reduction, and wind tunnel corrections can be found in the previous work.[47]

The Aero-Naut CAM carbon folding propellers were tested in a 2-blade configuration at rotation rates of 3,000 to 7,000 RPM and advancing flows of 8 to 80 ft/s, depending on the propeller and testing equipment limitations. Figure 12 provides an example propeller performance polars for the Aeronaut CAM 13x6.5 propeller, which was used on the UIUC-TUM Solar Flyer from 2017 to 2020. It was observed that Aero-Naut CAM carbon folding propeller blade geometry varied among propellers of the same diameter with different pitch values and among propellers of identical pitch-to-diameter ratios with different diameters. This geometry difference results in unique performance data for each propeller, therefore requiring individual performance testing of all propellers of interest. It was also found that increasing the pitch of a given diameter of propeller increases the non-dimensional performance and efficiency of the propeller, while shifting these characteristics toward higher advance ratios. The performance and efficiency increases continue with pitch until the propeller pitch-to-diameter ratio reaches approximately 0.8 to 1.0, after which the increase stabilizes, flattens over larger advance ratios, and sometimes then decreases. Similarly, for static conditions (zero velocity), increased propeller pitch increases thrust and power coefficients. Finally, Reynolds number effects were observed, with performance and efficiency increasing as RPM increases until a sufficiently high RPM is reached where there is marginal continued gain. The data produced, which is available for download on the UIUC Propeller Data Site[48] and on the Unmanned Aerial Vehicle Database,[49] will be used in the subsequent sections to optimize the propulsion system of the UIUC-TUM Solar Flyer.

American Institute of Aeronautics and Astronautics

(a)

(b)

(c)
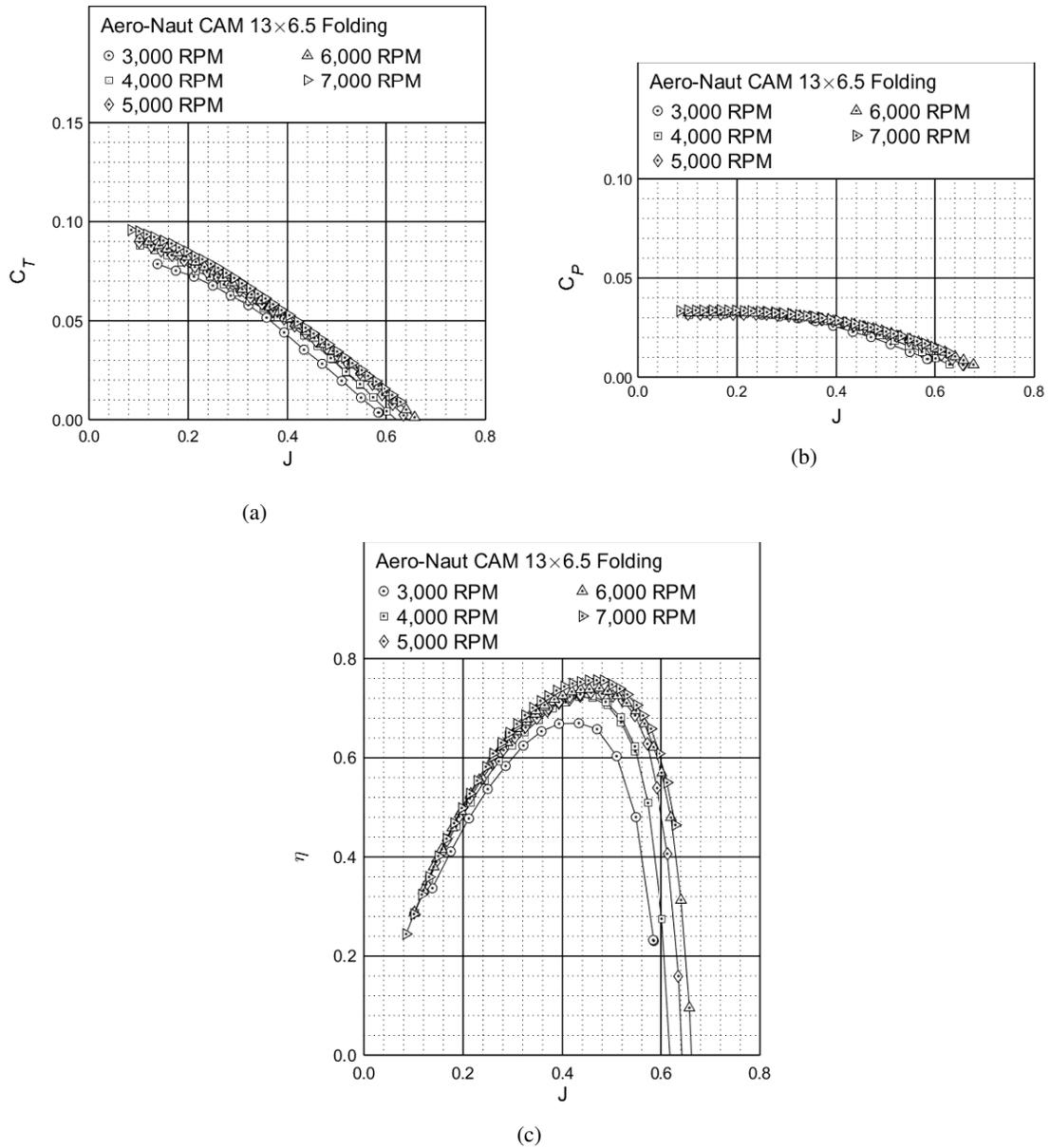
Figure 12: Propeller performance curves for the Aeronaut CAM 13x6.5 propeller used on the UIUC-TUM Solar Flyer from 2017 to 2020: (a) thrust (C_T), (b) power (C_P), and (c) efficiency $(\eta_{propeller})$ vs. advance ratio (J)

IV.   Mission Profile Simulation

The UIUC-TUM Solar Flyer is currently in development in order to perform applications that require continuous acquisition and processing of high resolution imagery. Along these lines, a key application task that stands out is wide area survey, which could be applied to a variety of applications; e.g. precision farming, infrastructure and environment monitoring, surveillance, surveying and mapping, search and rescue, etc. In order to optimize the aircraft propulsion system, a 1 km by 1 km field coverage flight is used as an example desired mission profile as it is indicative for the aforementioned applications. A trajectory plot of the mission is presented in Fig. 13.

The mission begins with a takeoff, followed by a 7.5 degree climb to 40 m in altitude. The aircraft then turns toward the desired area and flies approximately 400 m. It then maneuvers and proceeds to fly a field coverage pattern with 50 m radius turn-arounds after each pass; note that the turn radius is set by the desired ground coverage per related computational modeling work.[45] Thus, the field is covered with 11 passes, after which point the aircraft flies back toward the runway, maneuvers, and finally descends. The entire mission is flown at 10 m/s with exception of the climb out after takeoff; through flight testing of the UIUC-TUM Solar Flyer, this airspeed has been found to be most suitable for the aircraft to achieve efficient flight.

The resulting simulated state data for position, Euler angles, and velocity are presented in Fig. 14. The figure also contains thrust requirement predictions generated by the aforementioned aircraft power model,[35] using constants derived from aircraft specifications and previous flight tests.[32] As can be seen in the plot, with the exception of takeoff and landing, the aircraft consistently requires approximately 1.3 N to fly at 10 m/s. Due to the high efficiency of the airframe and the low-banked (11 deg) angle turns, the thrust requirement is approximately constant throughout the flight trajectory; the negligible increase in thrust required in these turns is consistent with the classical flight mechanics relation for constant bank-angle turns,[58] i.e. the increase follows $1/\cos(\phi) - 1$, yielding an increase of 1.9% for a 11 deg banked turn. This observation permits the aircraft thrust requirement to be set as a fixed value for all trajectories with a flight speed of 10 m/s, turn radii of at least 50 m, and constant altitude. Therefore, the optimization for the propulsion system of the UIUC-TUM Solar Flyer should be performed for a thrust of 1.3 N at a flight velocity of 10 m/s design point; this optimization is conducted in the following section.
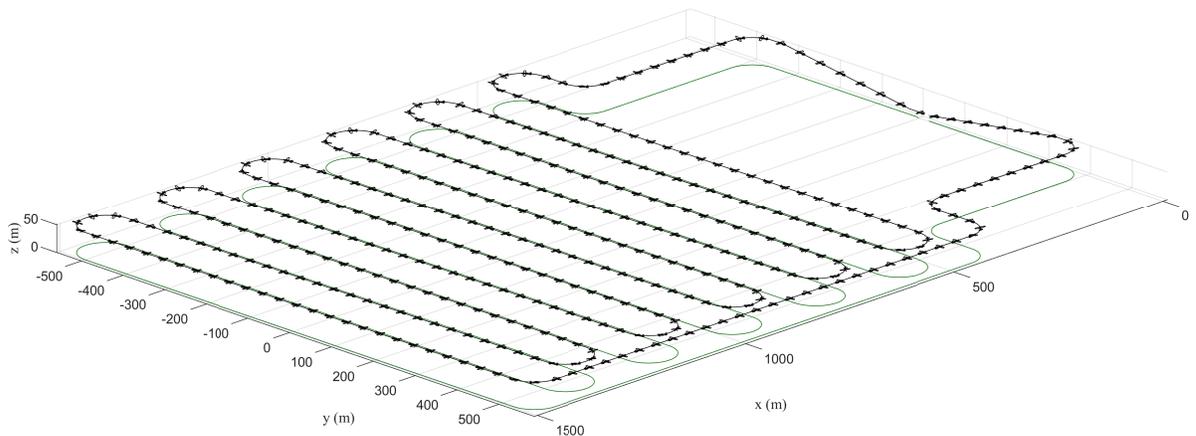
Figure 13: Trajectory plot of the simulated 1 km by 1 km field coverage flight mission (the aircraft is plotted every 4 s).
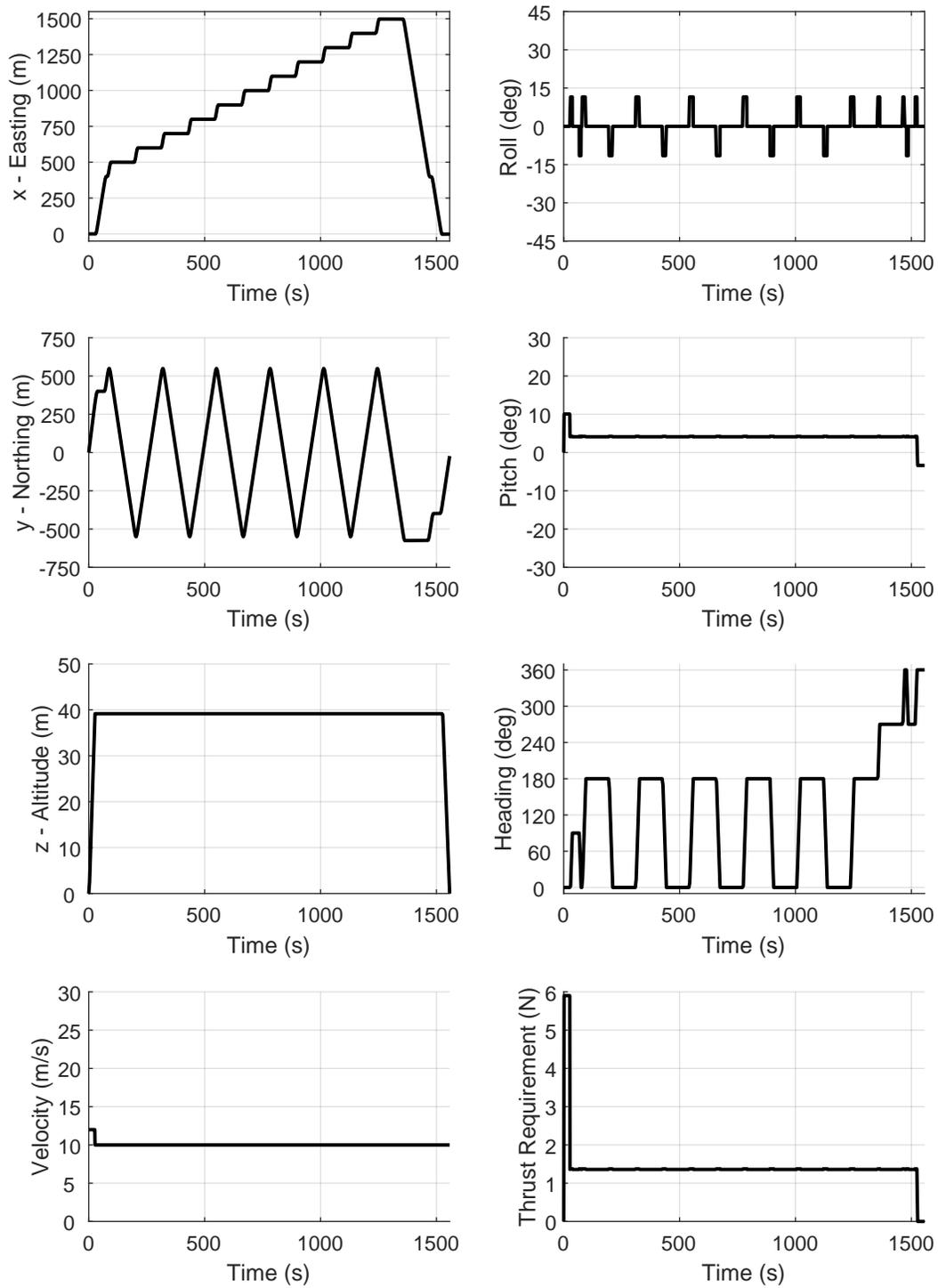
Figure 14: A time history of the simulated 1 km by 1 km field coverage flight mission.

V. Propulsion System Optimization

The propulsion system optimization tool was applied to the simulation results for the UIUC-TUM Solar Flyer that were presented in the previous section. Specifically, the tool was used to determine the optimal motor-propeller combination that would produce a thrust of 1.3 N at a flight velocity of 10 m/s; note that the propulsion system voltage was set at 12.0 V. The propulsion optimization tool used the propeller performance data for the 40 Aero-Naut CAM carbon folding propellers presented in Section III and motor parameters for 28 motors from Hacker Motor GmbH,[65] Model Motors s. r. o.,[66] and Neutronics;[67] the motors used were constrained to those that could geometrically fit within the nose of the UIUC-TUM Solar Flyer, that are less than 150 gr (such that the aircraft center of gravity is maintained), and that are regularly stocked and available for purchase (i.e. not custom-windings). In total, 1120 combinations were computed and ranked by the efficiency.

The motor-propeller optimization results are summarized below in Table 2 with the cells being shaded from green to red to indicate the efficiency. Note that only the top 144 combinations are presented in the table, correlating to the most efficient motor and propeller combinations for the desired thrust of 1.3 N at a flight velocity of 10 m/s — the remaining motors and propellers were less efficient for that design point.

Several key observations are made about the propulsion system optimization results. First, the baseline Model Motors AXi Cyclone 46/760 and Aero-Naut CAM 13x6.5 combination, which were used on the UIUC-TUM Solar Flyer from 2017 to 2020, had a combined efficiency of 55.2%. This combination ranked 150, meaning that although it was selected using radio control hobbyist experience for a broad range of thrusts and velocities, it has a relatively high efficiency at the desired 1.3 N of thrust and 10 m/s velocity.

Next, for the desired thrust and velocity, two propellers stand out as having the greatest efficiency: Aero-Naut CAM 12x8 followed by the Aero-Naut CAM 11x8, independent of motor chosen. These propellers were 5 to 15% relatively more efficient than the other propellers presented in the table. However, it should be noted that these two propellers

Table 2: Propulsion system optimization efficiency results for the UIUC-TUM Solar Flyer operating at velocity of 10 m/s with 1.3 N of thrust; note that only the most efficient 144 combinations are presented.

Propellers / Motors	Aero-Naut Modellbau GmbH CAM Carbon Folding								Efficiency (%)
	13x6.5	12.5x9	12.5x7.5	12x9	12x8	11x8	11x7	10x8	
Model Motors s.r.o. AXI Cyclone 46/760	55.2	53.8	56.4	53.2	57.3	56.3	55.0	52.6	65
25/1035	58.4	54.5	58.3	53.5	61.0	60.1	58.9	56.2	64
25/840	59.2	54.8	58.8	53.6	61.8	61.0	59.8	57.0	63
550/1200	53.8	50.2	53.6	49.2	56.1	55.3	54.2	51.8	62
550/720	56.7	52.5	56.3	51.4	59.2	58.5	57.3	54.7	61
480/1380	60.4	55.5	59.7	54.1	63.3	62.5	61.3	58.4	60
480/840	59.3	54.1	58.5	52.8	62.1	61.4	60.2	57.4	59
Hacker GmbH In-runners B40-26L-4:1PG	57.9	54.9	58.3	54.0	60.4	59.4	58.1	55.4	58
B40-22L-4:1PG	57.3	54.5	57.8	53.7	59.7	58.8	57.5	54.8	57
B40-20L-4:1PG	57.1	54.2	57.5	53.3	59.5	58.6	57.3	54.6	56
B40-18L-4:1PG	56.9	53.8	57.2	53.0	59.3	58.4	57.1	54.4	55
B40-15L-4:1PG	56.6	53.6	57.0	52.8	58.9	58.0	56.8	54.1	54
Neutronics Neu Motors 1110/1.5Y	62.8	57.7	62.2	56.5	65.8	65.0	63.6	60.6	53
1110/1Y	62.8	57.7	62.2	56.4	65.8	64.9	63.6	60.6	52
1110/1.5D	61.6	56.2	60.8	54.9	64.5	63.8	62.5	59.5	51
1107/2.5Y	62.4	56.3	61.2	54.9	65.4	64.7	63.5	60.4	50
1107/2Y	62.4	56.3	61.2	54.9	65.5	64.8	63.5	60.5	49
1105/3Y-4.4:1PG	60.1	58.5	61.4	57.9	62.5	61.4	59.9	57.1	48

produced 10 to 20% less maximum thrust at the UIUC-TUM Solar Flyer stall speed of 8 m/s than the larger Aero-Naut CAM 13x6.5 and Aero-Naut CAM 12.5x7.5. Therefore, the propellers with greater efficiency have a trade-off of providing less thrust for upset recovery.

For the thrust and velocity design point, it was found that the Neutronics Neu Motors, specifically the Neu Motors 1110/1.5Y and 1110/1Y followed by the Neu Motors 1107/2.5Y and 1107/2Y had the greatest efficiency, independent of propeller. The next best performing motors were the Neu Motors 1110/1.5D, the Model Motors AXi Cyclone 480/1380, the Neu Motors 1105/3Y with 4.4:1 planetary gearbox, and the Model Motors Cyclone AXi 480/840; however the specific order depended on the propellers they were matched with. These motors were 5 to 15% relatively more efficient than the remaining motors presented in the table; the remaining motors had similar efficiency to the aforementioned baseline Model Motors AXi Cyclone 46/760.

Finally, the motor-propeller combinations with the greatest efficiency for the 1.3 N thrust at 10 m/s velocity design point are the Neu Motors 1110/1.5Y and Aero-Naut CAM 12x8 and the Neu Motors 1110/1Y and Aero-Naut CAM 12x8; their efficiencies are 65.79% and 65.77%, respectively. These motor-propeller combinations are approximately 19% relatively more efficient than the baseline combination. The next most efficient motor-propeller combinations generally follow the order of the most efficient motors and most efficient propellers, individually mentioned above.

It is important to note that the combinations with the greatest efficiency must be strictly current-limited to prevent overheating and damaging the motor. Based on the motor speed constant and propulsion system voltage, the maximum rotation speed will draw significantly more current than permissible for these motors given the propeller matchings. Therefore, the motors can be operated very efficiently at and near the optimized set point conditions, however, should not be allowed to operate at full 'throttle', where the motors would certainly burn out.

VI.   Summary and Future Work

This paper described the propulsion system optimization of a computationally-intensive, long-endurance solar-powered unmanned aircraft, the UIUC-TUM Solar Flyer. Specifically, using a previously-developed fixed-wind, electric unmanned aircraft propulsion system power model and mission-based propulsion system optimization tool, a typical aircraft mission profile was simulated and the resulting thrust and velocity requirements were used to optimally-match propulsion system components, i.e. the propeller and motor, to maximize propulsion system efficiency. Using the methodology described in the paper, optimally-matched motor-propeller combinations were found that were 19% more efficient relative to the baseline combination used for the mission thrust and velocity design point. Additional improved efficiency matches were also presented that traded-off some efficiency gains (only 14% compared to the baseline combination) for increased thrust available in upset conditions (10 to 20% more thrust at stall speed).

For future work, the optimally-matched propeller-motor combination(s) will be installed on the UIUC-TUM Solar Flyer. The aircraft will then be flight tested to experimentally validate the propulsion system efficiency. Effort will also be allocated to qualitatively evaluated the upset recovery characteristics of the aircraft with each propeller-motor combination. After selecting an optimal propeller-motor combination for the UIUC-TUM Solar Flyer, long-endurance flight testing is expected to begin.

Acknowledgments

American Institute of Aeronautics and Astronautics

References

[1] "Altavian," http://www.altavian.com/, Accessed May 2020.

[2] Precision Hawk, "Precision Agriculture, Commercial UAV and Farm Drones," http://precisionhawk.com/, Accessed May 2020.

[3] MicroPilot, "MicroPilot - MP-Vision," http://www.micropilot.com/products-mp-visione.htm, Accessed May. 2015.

[4] Green, C. R. and McDonald, R. A., "Modeling and Test of the Efficiency of Electronic Speed Controllers for Brushless DC Motors," AIAA Paper 2015-3191, AIAA Aviation Forum, Dallas, TX, Jun. 2015.

[5] McCrink, M. H. and Gregory, J. W., "Blade Element Momentum Modeling for Low-Re Small UAS Electric Propulsion Systems," AIAA Paper 2015-3191, AIAA Aviation Forum, Dallas, TX, Jun. 2015.

[6] Lundstrom, D., Amadori, K., and Krus, P., "Validation of Models for Small Scale Electric Propulsion Systems," AIAA Paper 2010-483, AIAA Aerospace Sciences Meeting, Orlando, FL, Jan. 2010.

[7] McDonald, R. A., "Modeling of Electric Motor Driven Propellers for Conceptual Aircraft Design," AIAA Paper 2015-1676, AIAA Aerospace Sciences Meeting, Kissimmee, Florida, Jan. 2015.

[8] Brandt, J. B., *Small-Scale Propeller Performance at Low Speeds*, Master's thesis, University of Illinois at Urbana-Champaign, Department of Aerospace Engineering, Urbana, IL, 2005.

[9] Brandt, J. B. and Selig, M. S., "Propeller Performance Data at Low Reynolds Numbers," AIAA Paper 2011-1255, AIAA Aerospace Sciences Meeting, Orlando, FL, Jan. 2011.

[10] Lundstrom, D. and Krus, P., "Testing of Atmospheric Turbulence Effects on the Performance of Micro Air Vehicles," *International Journal of Micro Air Vehicles*, Vol. 4, No. 2, Jun. 2012, pp. 133–149.

[11] Lindahl, P., Moog, E., and Shaw, S. R., "Simulation, Design, and Validation of an UAV SOFC Propulsion System," *IEEE Transactions on Aerospace and Electronic Systems*, Vol. 48, No. 3, Jul. 2012, pp. 2582–2593.

[12] Uhlig, D. V., *Post Stall Propeller Behavior at Low Reynolds Numbers*, Master's thesis, University of Illinois at Urbana-Champaign, Department of Aerospace Engineering, Urbana, IL, 2007.

[13] Uhlig, D. V. and Selig, M. S., "Post Stall Propeller Behavior at Low Reynolds Numbers," *AIAA Paper 2008-407, AIAA Aerospace Sciences Meeting, Reno, Nevada, Jan. 2008*.

[14] Deters, R. W. and Selig, M. S., "Static Testing of Micro Propellers," AIAA Paper 2008-6246, AIAA Applied Aerodynamics Conference, Honolulu, Hawaii, Aug. 2008.

[15] Chaney, C. S., Bahrami, J. K., Gavin, P. A., Shoemake, E. D., Barrow, E. S., and Matveev, K. I., "Car-Top Test Module as a Low-Cost Alternative to Wind Tunnel Testing of UAV Propulsion Systems," *Journal of Aerospace Engineering*, Vol. 27, No. 6, Nov. 2014.

[16] Deters, R. W., *Performance and Slipstream Characteristics of Small-Scale Propelllers at Low Reynolds Numbers*, Ph.D. thesis, University of Illinois at Urbana-Champaign, Department of Aerospace Engineering, Urbana, IL, 2014.

[17] Deters, R. W., Kleinke, S., and Selig, M. S., "Static Testing of Propulsion Elements for Small Multirotor Unmanned Aerial Vehicles," AIAA Paper 2017-3743, AIAA Aviation Forum, Denver, CO, Jun. 2017.

[18] Dantsker, O. D., Selig, M. S., and Mancuso, R., " A Rolling Rig for Propeller Performance Testing," AIAA Paper 2017-3745, AIAA Applied Aerodynamics Conference, Denver, CO, Jun. 2017.

[19] Gong, A. and Verstraete, D., "Experimental Testing of Electronic Speed Controllers for UAVs," AIAA Paper 2017-4955, AIAA/SAE/ASEE Joint Propulsion Conference, Atlanta, GA, Jul. 2017.

[20] Gong, A., Maunder, H., and Verstraete, D., "Development of an in-fight thrust measurement system for UAVs," AIAA Paper 2017-5092, AIAA/SAE/ASEE Joint Propulsion Conference, Atlanta, GA, Jul. 2017.

[21] Gong, A., MacNeill, R., and Verstraete, D., "Performance Testing and Modeling of a Brushless DC Motor, Electronic Speed Controller and Propeller for a Small UAV," AIAA Paper 2018-4584, AIAA Propulsion and Energy Forum, Cincinnati, OH, Jul. 2018.

[22] Deters, R. W., Dantsker, O. D., Kleinke, S., Norman, N., and Selig, M. S., "Static Performance Results of Propellers Used on Nano, Micro, and Mini Quadrotors," AIAA Paper 2018-4122, AIAA Aviation Forum, Atlanta, GA, Jun. 2018.

[23] Drela, M., "DC Motor / Propeller Matching," http://web.mit.edu/drela/Public/web/qprop/motorprop.pdf, Accessed May 2020.

[24] Mark Drela, "QPROP," http://web.mit.edu/drela/Public/web/qprop/, Accessed Jan. 2019.

[25] Lundstrom, D., *Aircraft Design Automation and Subscale Testing*, Ph.D. thesis, Linkoping University, Department of Management and Engineering, Linkoping, Sweden, 2012.

[26] McDonald, R. A., "Modeling of Electric Motor Driven Variable Pitch Propellers for Conceptual Aircraft Design," AIAA Paper 2016-1025, AIAA Aerospace Sciences Meeting, San Diego, California, Jan. 2016.

[27] MacNeill, R., Verstraete, D., and Gong, A., "Optimisation of Propellers for UAV Powertrains," AIAA Paper 2017-5090, AIAA/SAE/ASEE Joint Propulsion Conference, Atlanta, GA, Jul. 2017.

[28] Macneill, R. and Verstraete, D., "Optimal Propellers for a Small Hybrid Electric Fuel-Cell UAS," AIAA Paper 2018-4981, AIAA/IEEE Electric Aircraft Technologies Symposium, Cincinnati, OH, Jul. 2018.

[29] Theile, M., Dantsker, O. D., Caccamo, M., and Yu, S., "uavAP: A Modular Autopilot Framework for UAVs," AIAA Paper 2020-3268, AIAA Aviation 2020 Forum, Virtual Event, Jun. 2020.

[30] Al Volo LLC, "Al Volo: Flight Systems," http://www.alvolo.us, Accessed Jun. 2020.

[31] Dantsker, O. D., Theile, M., Caccamo, M., and Mancuso, R., "Design, Development, and Initial Testing of a Computationally-Intensive, Long-Endurance Solar-Powered Unmanned Aircraft," AIAA Paper 2018-4217, AIAA Applied Aerodynamics Conference, Atlanta, GA, Jun. 2018.

[32] Dantsker, O. D., Theile, M., Caccamo, M., Yu, S., Vahora, M., and Mancuso, R., "Continued Development and Flight Testing of a Long-Endurance Solar-Powered Unmanned Aircraft: UIUC-TUM Solar Flyer," AIAA Paper 2020-0781, AIAA Scitech 2020 Forum, Orlando, FL, Jan. 2020.

[33] Real Time and Embedded System Laboratory, University of Illinois at Urbana-Champaign, "Solar-Powered Long-Endurance UAV for Real-Time Onboard Data Processing," http://rtsl-edge.cs.illinois.edu/UAV/, Accessed Jan. 2018.

[34] Dantsker, O. D., Imtiaz, S., and Caccamo, M., "Electric Propulsion System Optimization for a Long-Endurance and Solar-Powered Unmanned Aircraft," AIAA Paper 2019-4486, AIAA/IEEE Electric Aircraft Technology Symposium, Indianapolis, Indiana, Aug. 2019.

[35]Dantsker, O. D., Theile, M., and Caccamo, M., "A High-Fidelity, Low-Order Propulsion Power Model for Fixed-Wing Electric Unmanned Aircraft," AIAA Paper 2018-5009, AIAA/IEEE Electric Aircraft Technologies Symposium, Cincinnati, OH, Jul. 2018.

[36]Lee, J. S. and Yu, K. H., "Optimal Path Planning of Solar-Powered UAV Using Gravitational Potential Energy," *IEEE Transactions on Aerospace and Electronic Systems*, Vol. 53, No. 3, Jun. 2017, pp. 1442–1451.

[37]Grano-Romero, C., García-Juárez, M., Guerrero-Castellanos, J. F., Guerrero-Sánchez, W. F., Ambrosio-Lázaro, R. C., and Mino-Aguilar, G., "Modeling and control of a fixed-wing UAV powered by solar energy: An electric array reconfiguration approach," *2016 13th International Conference on Power Electronics (CIEP)*, Jun. 2016, pp. 52–57.

[38]Gao, X.-Z., Hou, Z.-X., Guo, Z., Liu, J.-X., and Chen, X.-Q., "Energy management strategy for solar-powered high-altitude long-endurance aircraft," *Energy Conversion and Management*, Vol. 70, No. Supplement C, 2013, pp. 20 – 30.

[39]Hosseini, S., Dai, R., and Mesbahi, M., "Optimal path planning and power allocation for a long endurance solar-powered UAV," *2013 American Control Conference*, Jun. 2013, pp. 2588–2593.

[40]B. Lee, B., Park, P., Kim, C., Yang, S., and Ahn, S., "Power managements of a hybrid electric propulsion system for UAVs," *Journal of Mechanical Science and Technology*, Vol. 26, No. 8, Aug 2012, pp. 2291–2299.

[41]Ostler, J. and Bowman, W., "Flight Testing of Small, Electric Powered Unmanned Aerial Vehicles," U.S. Air Force T&E Days Conferences, American Institute of Aeronautics and Astronautics, Dec. 2005.

[42]Karabetsky, D., "Solar rechargeable airplane: Power system optimization," *2016 4th International Conference on Methods and Systems of Navigation and Motion Control (MSNMC)*, Oct. 2016, pp. 218–220.

[43]Park, H. B., Lee, J. S., and Yu, K. H., "Flight evaluation of solar powered unmanned flying vehicle using ground testbed," *2015 15th International Conference on Control, Automation and Systems (ICCAS)*, Oct. 2015, pp. 871–874.

[44]Shiau, J. K., Ma, D. M., Chiu, C. W., and Shie, J. R., "Optimal Sizing and Cruise Speed Determination for a Solar-Powered Airplane," *AIAA Journal of Aircraft*, Vol. 47, No. 2, Mar. 2010, pp. 622–629.

[45]Dantsker, O. D., Theile, M., and Caccamo, M., "Integrated Power Modeling for a Solar-Powered, Computationally-Intensive Unmanned Aircraft," AIAA Paper 2020-3568, AIAA/IEEE Electric Aircraft Technology Symposium, Virtual Event, Aug. 2020.

[46]Ol, M., Zeune, C., and Logan, M., "Analytical/Experimental Comparison for Small Electric Unmanned Air Vehicle Propellers," *26th AIAA Applied Aerodynamics Conference*, American Institute of Aeronautics and Astronautics, Reston, VA, 8 2008.

[47]Dantsker, O. D., Caccamo, M., Deters, R. W., and Selig, M. S., "Performance Testing of Aero-Naut CAM Folding Propellers," AIAA Paper 2020-2762, AIAA Aviation 2020 Forum, Virtual Event, Jun. 2020.

[48]UIUC Applied Aerodynamics Group, "UIUC Propeller Data Site," http://m-selig.ae.illinois.edu/props/propDB.html.

[49]O. Dantsker and R. Mancuso and M. Vahora and M. Caccamo, "Unmanned Aerial Vehicle Database," http://uavdb.org/.

[50]Drela, M., "First-Order DC Electric Motor Model," http://web.mit.edu/drela/Public/web/qprop/motor1_theory.pdf, Accessed May 2020.

[51]Drela, M., "Second-Order DC Electric Motor Model," http://web.mit.edu/drela/Public/web/qprop/motor2_theory.pdf, Accessed May 2020.

[52]Mancuso, R., Dantsker, O. D., Caccamo, M., and Selig, M. S., "A Low-Power Architecture for High Frequency Sensor Acquisition in Many-DOF UAVs," Submitted to International Conference on Cyber-Physical Systems, Berlin, Germany, April 2014.

[53]Dantsker, O. D., Mancuso, R., Selig, M. S., and Caccamo, M., "High-Frequency Sensor Data Acquisition System (SDAC) for Flight Control and Aerodynamic Data Collection Research on Small to Mid-Sized UAVs," AIAA Paper 2014-2565, AIAA Applied Aerodynamics Conference, Atlanta, GA, Jun. 2014.

[54]Dantsker, O. D., *Measurement of Unsteady Aerodynamic Characteristics of a Subscale Aerobatic Aircraft in High Angle-of-Attack Maneuvers*, Master's thesis, University of Illinois at Urbana-Champaign, Department of Aerospace Engineering, Urbana, IL, 2015.

[55]Dantsker, O. D., Yu, S., Vahora, M., and Caccamo, M., "Flight Testing Automation to Parameterize Unmanned Aircraft Dynamics," AIAA Paper 2019-3230, AIAA Aviation and Aeronautics Forum and Exposition, Dallas, TX, Jun. 2019.

[56]Theile, M., Dantsker, O. D., Nai, R., and Caccamo, M., "uavEE: A Modular, Power-Aware Emulation Environment for Rapid Prototyping and Testing of UAVs," IEEE International Conference on Embedded and Real-Time Computing Systems and Applications, Hakodate, Japan, Aug. 2018.

[57]Landing Products Inc., "APC Propellers," https://www.apcprop.com/, Accessed May 2020.

[58]Yechout, T. R., Morris, S. L., Bossert, D. E., Hallgren, W. F., and Hall, J. K., *Introduction to Aircraft Flight Mechanics, 2nd Edition*, American Institute of Aeronautics and Astronautics, Inc., Reston, VA, 2014.

[59]aero-naut Modellbau GmbH & Co. KG, "CAMcarbon folding propellers," http://www.aero-naut.de/en/products/airplanes/accessories/propellers/camcarbon-folding-prop/, Accessed May 2020.

[60]Lockheed Martin Corporation, "Stalker XE UAS," https://www.lockheedmartin.com/en-us/products/stalker.html, Accessed May 2020.

[61]Silent Falcon UAS Technologies, "Silent Falcon," http://www.silentfalconuas.com/silent-falcon, Accessed May 2020.

[62]Zipline International, "Zipline - Lifesaving Deliveries by Drone," https://flyzipline.com/, Accessed May 2020.

[63]Israel Aerospace Industries Ltd., "Military Malat Products Bird Eye 400," http://www.iai.co.il/2013/36943-34720-en/Bird_Eye_Family.aspx, Accessed May. 2019.

[64]Deters, R. W., Ananda, G. K., and Selig, M. S., "Reynolds Number Effects on the Performance of Small-Scale Propellers," AIAA Paper 2014-2151, AIAA Applied Aerodynamics Conference, Atlanta, GA, Jun. 2014.

[65]Hacker Motor GmbH, "Hacker Brushless Motors," https://www.hacker-motor.com/, Accessed Aug. 2020.

[66]Model motors s.r.o., "AXI Model Motors," http://www.modelmotors.cz/, Accessed Aug. 2020.

[67]Neutronics, "NeuMotors," https://neumotors.com/, Accessed Aug. 2020.

American Institute of Aeronautics and Astronautics